SnO_2-embedded nanoporous carbon electrode with reaction-buffer space for stable all-solid-state Li ion battery

Hiroo Notohara, Koki Urita, Isamu Moriguchi*

Graduate School of Engineering, Nagasaki University, 1-14 Bunkyo-machi, Nagasaki 852-8521, Japan

KEYWORDS. All-solid-state battery, Li-ion battery, Nanoporous carbon, Tin dioxide, Nanocomposite

ABSTRACT: The conventional approach for fabricating all-solid-state batteries has required highly dense layer of electrode and electrolyte. Their close contact interface is not suitable for alloy- or conversion-based active materials because their large volume change in lithiation/delithiation reactions causes a collapse of the contact interface or reaction limitations under mechanical constriction. In this study, we propose that a SnO_2-embedded porous carbon electrode shows high cyclability and high capacity even at high constraint pressure owing to the nanopores which work as a buffer space for the large volume change accompanied with SnO_2-Sn conversion reaction and Sn-Li alloying-dealloying reaction. A detailed investigation between structural parameters of the electrode material and charge-discharge properties revealed Li ion conduction in carbon nanopores from solid electrolyte located the outside as well as the optimal conditions to yield high performance. 75 wt% of SnO_2 loading in carbon nanopores, which provides the buffer space corresponding to the inevitable volume expansion by full lithiation, brought out excellent performance at room temperature superior to that in an organic liquid electrolyte system: high capacity of 1023 mAh/g-SnO_2 at 50 mA/g, high capacity retention of 97 % at 300th cycle at 300 mA/g and high rate capability with over 75 % capacity retention at 1000 mA/g against 50 mA/g, whose values are also superior to the system using the organic liquid electrolyte.

1. Introduction

All-solid-state lithium ion batteries (ASS-LIBs) are expected as one of promised energy storage devices by the characteristics of safety and high energy density. The recently discovered sulfide-based solid electrolyte(SE) has high ionic conductivity over 10^{-3} S/cm at room temperature, [1-3] and it has been accelerated the development of a high capacity bulk-type cell of ASS-LIB applicable to electric vehicles, power grid systems and so on. On conventional research, highly dense electrode layer with close contact interface has been fabricated to ensure sufficient Li ion conductive interface in electrode layer and SE layer.[4, 5] However, application of high capacity active material such as Si, Sn, Ge, P, SnO_2 and so on[6] to the ASS-LIB system has a serious problem of interfacial collapse causing capacity degradation during charge-discharge cycling due to the large volume change which is accompanied by alloying-dealloying reaction and conversion reaction. Although the increase in external cell constraint pressure is effective to suppress the interfacial collapse, the capacity was decreased because of the limitation of reactions accompanied with volume change.[7-9] In order to achieve high cyclability and high capacity on ASS-LIB, it is important to design the electrode structure providing a reaction space while keeping a stable contact of SE/electrode interface.

Various synthesis methods for metal/carbon composite materials have been reported.[10-13] These composites are promising for the development of lithium and sodium ion storage on ASS system. We found recently that SnO_2 nanocrystallites embedded in nanopores of porous carbons were able to react with Li ions diffused from SE located outside of the pores.[14] We also succeeded in the development of a prototype ASS-LIB cell using a negative electrode composed of SnO_2/porous carbon composite and SE, which showed high capacity and good cycle stability. The porous electrode used to be considered not to be applicable as ASS battery electrode materials because of the difficulty to make enough Li ion conduction path and its low volumetric energy density. However, the active material/porous carbon composite electrode with nanopores working as a buffer space for the volume change proposed a new approach to fabricating a stable electrode/SE interface in bulk-type cell without electrode expansion. High performance electrode will be developed by designing porous composite structure with optimal pore space considering the inevitable volume expansion of lithiated active materials.

The present work has investigated an ideal reaction-buffer space on ASS-LIBs from relationship between charge-discharge properties and the structure of SnO_2/porous carbon composite electrode as well as the external cell constraint pressure. We have disclosed that the optimization of SnO_2 loading amount in carbon nanospace, pore volume and constraint pressure. The SnO_2 embedded porous carbon composite with optimal electrode structure showed high capacity, high cyclability and high rate performance relative to those of the cell using organic liquid electrolyte (OLE).

2. EXPERIMENTAL SECTION

2.1 Chemicals. 37 wt% aqueous formaldehyde and phenol purchased from Kishida Chemical Co. Ltd (guaranteed regent) were used as carbon source. SiO_2 colloidal solutions (average particle diameter: 45 and 140 nm) were obtained from JGC Catalysts and Chemicals Ind. Co. Ltd. (Cataloid series SI-45P and SS-140). $SnCl_2$ was purchased from Kishida Chemical Co. Ltd.

(extra pure regent), and was used for the source of SnO_2 embedded in porous carbons. SnO_2 particles-dispersive methanol solution was obtained from Nissan Chemical Co. Ltd. (CELNAX CX-S501) to prepare an electrode mixing SnO_2 nanoparticles with acetylene black. All of them were used without additional purification. We used the following commercial materials for electrochemical measurements: Li metal foil (0.1 nm in thickness, Honjo Metal Co. Ltd.), In metal foil (0.1 nm in thickness, Nilaco Co. Ltd.), acetylene black (AB, Denki Kagaku Kogyo K.K.), Poly(vinylidene difluoride) (PVdF, Kureha Co. Ltd.) and a 1.0 mol dm^{-3} solution of $LiPF_6$ in ethylene carbonate/dimethyl carbonate (1/1 by volume) (Kidhida Chemical Co. Ltd.). Li_2S (99.98%), P_2S_5 (99%) and LiI (99.9%), which were used the precursor of solid electrolyte, were purchased from Sigma Aldrich Co. LLC.

2.2 Synthesis and structural analyses of SnO_2/nanoporous carbon composites. SnO_2 nanocrystallites were embedded into nanopores of a silica opal-derived porous carbon (C*X*; *X* is an average diameter of 140 nm and 45 nm) by thermal process and a subsequent hydrolysis.[11] A mixture of $SnCl_2$ and C*X* was heated in a sealed glass tube at 593 K for 24 hours, and the embedded $SnCl_2$ was hydrolyzed by water and dried in *vacuo*. The weight % of $SnCl_2$ introducing into pores of C*X* was set from 40 to 97 to control the SnO_2-loading amount in the composite. The obtained composite here is named as SnO_2/C*X*[*w*], where *w* indicates weight % of the SnO_2 content in the composites determined by thermogravimetric analysis (TGA, SEIKO Instrument Inc., TG/DTA7300) under air flow up to 700 ˚C. The crystallite structures were examined from powder X-ray diffraction (XRD, Rigaku miniflex-600) using Cu Kα radiation. N_2 adsorption isotherms at 77 K (MicrotracBEL Co. Ltd., BELSORP-mini) were measured to determine specific surface area, total pore volume and pore size distribution by applying α_s-plot analysis,[15, 16] Brunauer-Emmett-Teller (BET) method and grand canonical Monte Carlo (GCMC) method, respectively. The surface morphology and the structure inside pores of samples were directly observed by scanning electron microscope (SEM, JEOL JSM-7500FAM) and scanning transmission electron microscope (HR-STEM, JEOL ARM-200CF). The bonding state of Sn compounds after initial discharge was examined by X-ray photoelectron spectroscopy (XPS, Shimazu Co. Ltd., AXIS-ULTRA DLD) using Al Kα radiation. As a reference composite sample (SnO_2·AB[*w*]), SnO_2 powder was obtained by drying the SnO_2 nanoparticles-dispersive methanol solution (CELNAX CX-S501), and then was mixed with AB in a mortar.

2.3 Cell fabrication and Electrochemical Measurements. The charge-discharge performance of SnO_2/C*X*[*w*] was measured by using a two electrode-type ASS cell. The detail procedure for preparation of glassy SE which is a mixture of LiI and $75Li_2S$-$25P_2S_5$[17] has already reported in the previous report.[14] The working electrode was obtained by dispersing SnO_2/C*X*[*w*] and SE with the volume ratio of 50:50 in heptane using a sonication and drying them in *vacuo* at room temperature. A half-cell was assembled in an Ar-filled glove box using a polycarbonate cylinder with the internal diameter of 13 mm as follows. After 135 mg of SE powder was pressed to form a SE pellet layer in the polycarbonate cylinder, a Li-In alloy foil was attached to one side of the SE layer as the counter electrode. The Li-In alloy foil was made from Li (8 mm in diameter) and In (10 mm in diameter) circular foils in advance by stacking and pressing at 70 MPa for 7 minutes at room temperature. The composition of LiIn alloy was Li/In = 0.73 in atomic ratio. 2 mg of the composite of SnO_2/C*X*[*w*] and SE was placed on the other side of SE layer as the working electrode layer. Small amount of working electrode material was used to evaluate the charge-discharge performance of the electrode active material itself. The stacked three-layer was sandwiched between two stainless-steel rods as current correctors, and then was finally pressed at 300 MPa for 5 minutes at room temperature using a uniaxial oil hydraulic press. The charge-discharge curves were examined by using an electrochemical analyzer (Hokuto Denko, HJ-SD8) at 25°C under a constant current (CC) mode; the specific current of 50 to 1000 mA/g based on the weight of SnO_2 in the potential range of –0.61 to 1.38 V vs. LiIn, corresponding to 0.01 − 2.0 V vs. Li. An external constraint pressure of 3.5, 6.3 or 9.1 MPa was applied on the ASS half-cell throughout the electrochemical measurements by using a vise. Electrochemical properties of SnO_2/C*X*[*w*] in an OLE was measured under same condition with previous reports.[10, 11] A working electrode of mixture of SnO_2/C*X*[*w*] and PVdF with the weight ratio of 9:1 coated on a Cu foil, a Li-metal counter electrode and a 1.0 mol dm^{-3} $LiPF_6$ in ethylene carbonate/dimethyl carbonate (1/1 by volume) were set in a CR2032 coin cell. The SE powder was not used in the OLE system.

3. Results and Discussion

3.1 Structural characteristics of SnO_2-embedded nanoporous carbons. It is important to provide composite samples with perfectly embedded SnO_2 in the carbon nanopores so as to evaluate the effect of buffer space and porous composite structure on the electrochemical property. SnO_2/C*X*[*w*] samples were provided here as listed in Table 1**,** where the structural parameters were characterized by XRD (Figure S1 in Supporting Information) and N_2 ad-/desorption isotherm (Figure S2 in Supporting Information) measurements. The primary crystallite size of SnO_2 deposited in these composites was estimated around 3 nm from (110) X-ray diffraction peak by the Scherrer equation. The specific pore volumes ($V_{comp.}$) and specific surface areas (S_a) were decreased with increasing SnO_2 loading amount in the composite (*w*). The pore size distribution of SnO_2/C*X*[*w*] was become smaller with the increasing the loading amount of SnO_2 (Figure S3 in Supporting Information). In

Table 1. Structural parameters of the samples.

	S_a (m^2/g)	$V_{comp.}$ (cm^3/g)	*w* (wt%)	$w_{calc.}$ (wt%)
SnO_2/C45[*w*]	1110	1.66	0	0
	497	0.89	38	43
	290	0.65	74	56
	242	0.41	82	73
SnO_2/C140[*w*]	1243	1.86	0	0
	623	0.67	37	59
	419	0.47	52	69
	188	0.38	65	74
	124	0.25	75	81
	49	0.17	83	84

S_a: specific surface area, $V_{comp.}$: specific pore volume, *w*: SnO_2 content measured, $w_{calc.}$: SnO_2 content estimated from the pore volume change (see in Supporting Information).

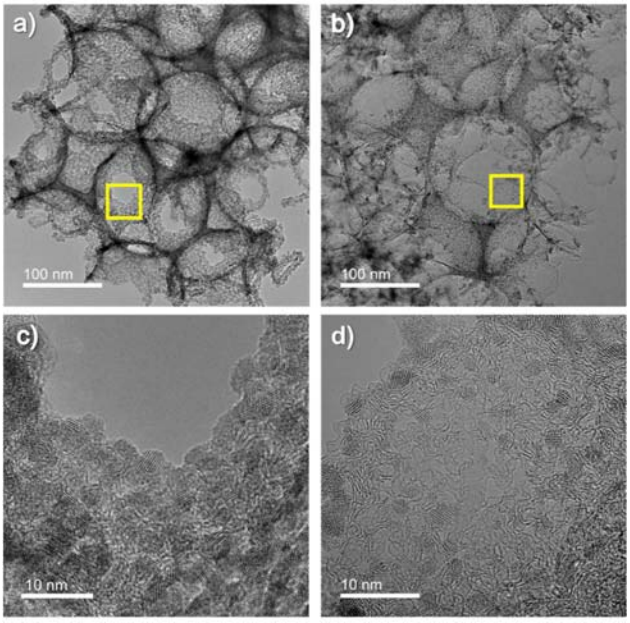

Figure 1. TEM images of (a) SnO_2/C140[75] and (b) SnO_2/C140[37]. (c,d) Enlarged images of yellow frame in (a) and (b), respectively.

addition, the loading amount of SnO_2 ($w_{calc.}$) estimated from the pore volume change between SnO_2/C*X*[*w*] and original C*X* almost agrees with the value of *w* determined from TG weight loss in air (Figure S4 and Supplementary Calculations in Supporting Information). These results indicate that SnO_2 are preferentially deposited in nanopores of porous carbons.

TEM observation demonstrated that SnO_2 nanocrystallites were deposited on the nanopore wall of C*X* as shown in Figure 1. The size of SnO_2 particles was corresponded to the crystallite size of 3 ~ 5 nm estimated by the XRD measurement. The SnO_2 nanocrystallites were densely accumulated in the nanopores for SnO_2/C140[75] with the highly SnO_2-loading (Figure 1a, c). In the case of low SnO_2 loading sample, they were highly dispersive on macropores of C140 (Figure 1b, d). Our previous study has already reported that the porous structure of SnO_2/C*X*[*w*] not filled with SE is maintained even after the cell construction with compressing process.[14]

3.2 Charge-discharge properties of SnO_2–embedded nanoporous carbons in ASS system. Figure 2 shows charging-discharging curves and their differential (d*Q*/d*V*) curves of SnO_2/C140[75] and SnO_2 ·AB [75] at 25 ˚C under the external cell constraint pressure of 9.1 MPa. Porous carbon electrodes often deliver an irreversible capacity due to a lot of oxygen-containing functional groups. The irreversible capacity in SnO_2/C140[75] should mainly stem from C140 (Figure S5(a) in Supporting Information).

SnO_2/C140[75] showed higher capacity and clearer d*Q*/d*V* peaks of dealloying reaction around –0.1 V vs. LiIn (0.5 V vs. Li) and conversion reaction around 0.5 V vs. LiIn (1.1 V vs. Li) than SnO_2·AB [75] in charging process. Especially, sharp d*Q*/d*V* peaks of conversion reaction were reproducibly observed on SnO_2/C140[75] in contrast to weak and broad peaks on SnO_2·AB [75], suggesting the suppression of polarization

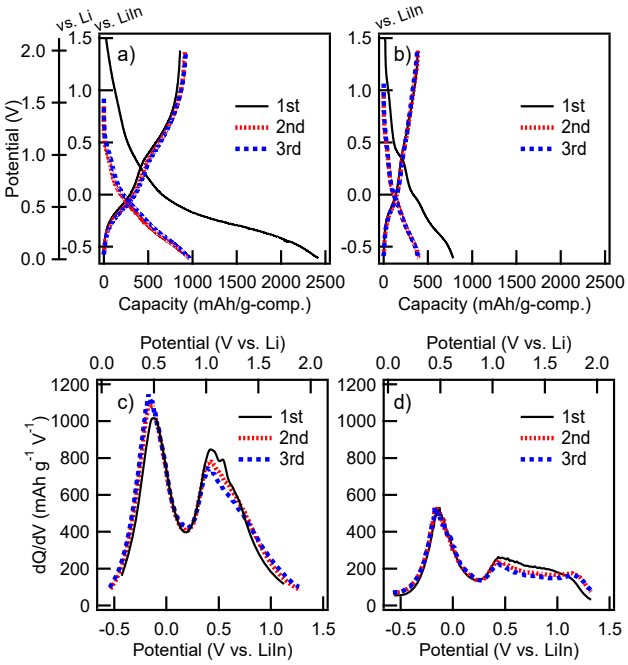

Figure 2. Charge-discharge curves during the initial three cycles of (a) SnO_2/C140[75] and (b) SnO_2·AB[75]. (c, d) d*Q*/d*V* curves of the charge curves in (a) and (b), respectively. The charge capacity is based on the weight of (a) SnO_2/C140[75] and (b) SnO_2· AB[75], respectively.

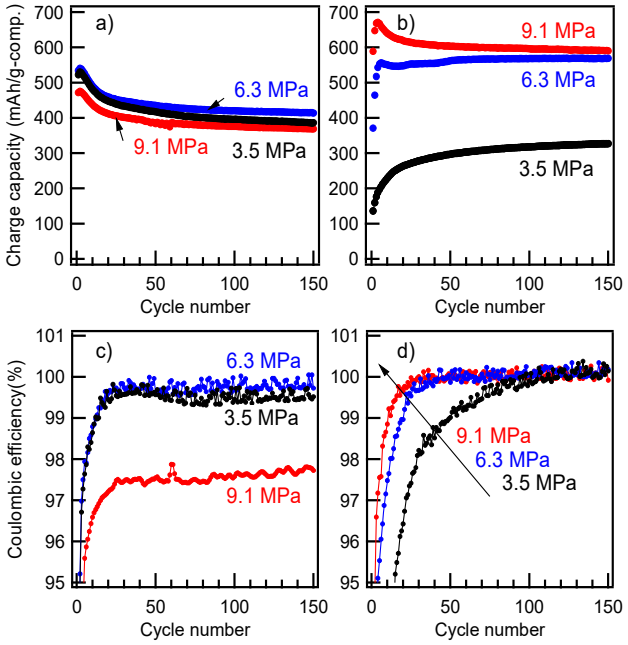

Figure 3. Effect of constraint pressure on (a, b) cycle performance and (c, d) coulombic efficiency of SnO_2 · AB[70] and SnO_2/C140[75] ; (a, c) SnO_2·AB[70], (b, d) SnO_2/C140[75]. The charge capacity is based on the weight of composite samples.

and improvement of reversibility of conversion reaction by embedding SnO_2 nanocrystallites in the carbon nanopores. The charge capacity of SnO_2/C140[75] after 3 cycles at the specific

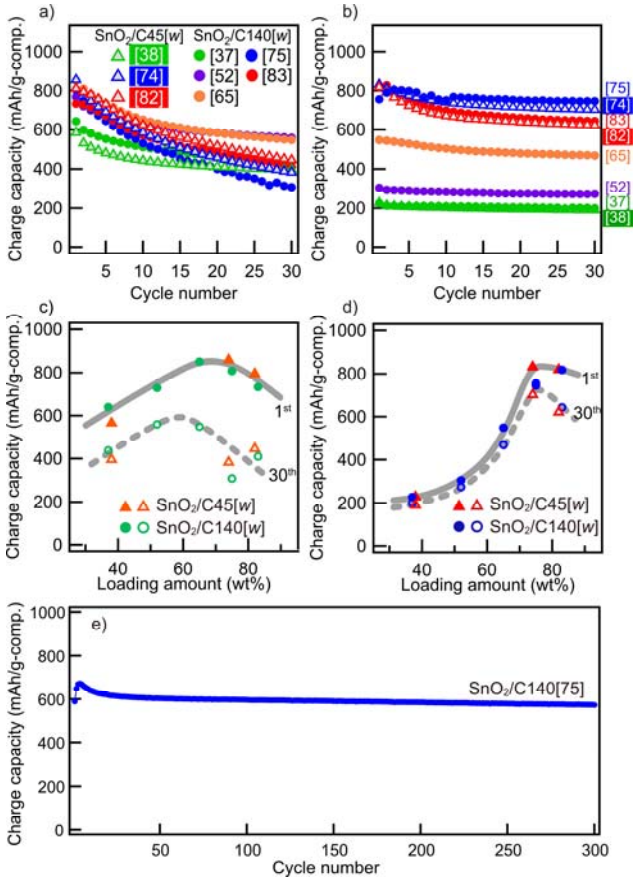

Figure 4. Charge capacities of SnO_2/C*X*[*w*] samples in (a, c) OLE and (b, d, e) ASS systems as functions of (a, b) cycle number and (c, d) loading amount of SnO_2. The numeral in brackets in (a, b) indicates the *w* value in SnO_2/C*X*[*w*]. Opened and closed symbols in (c) and (d) show the charge capacities at the 1st and 30th cycle, respectively. The charge capacity is based on the weight of composite (SnO_2/C*X*[*w*]) samples. The specific current of (a, b) and (e) were 50 mA/g-SnO_2 and 300 mA/g-SnO_2, respectively. The external pressure of 9.1 MPa was applied during charge-discharge test on the ASS system.

current of 50 mA/g was 1023 mAh/g based on SnO_2 weight. The SnO_2-based capacity was estimated by subtracting the capacity of C140 corresponding to its wt% in SnO_2/C140[75]. C140 showed a capacity of 140 mAh/g at the same condition, and no remarkable reactions around –0.1 V vs. LiIn and 0.5 V vs. LiIn were confirmed by the d*Q*/d*V* curves (Figure S5(b) in Supporting Information). Since the SnO_2-based capacity of SnO_2/C140 is higher than the theoretical capacities of 711 mAh/g and 781 mAh/g calculated from the conversion reaction and the alloying-dealloying reaction, both reactions are contributed on charge and discharge reaction.

Cycle performance of SnO_2/C140[75] and SnO_2·AB[70] was compared at the specific current of 300 mA/g under the external cell constraint pressure of 3.5, 6.3 and 9.1 MPa (Figure 3). The capacity and coulombic efficiency of SnO_2·AB [70] were slightly increased by increasing the constraint pressure from 3.5 to 6.3 MPa, but they were decreased at 9.1 MPa. Although highly dense electrode is required to yield effective ion and electron conductive paths in a general ASS battery, the volume

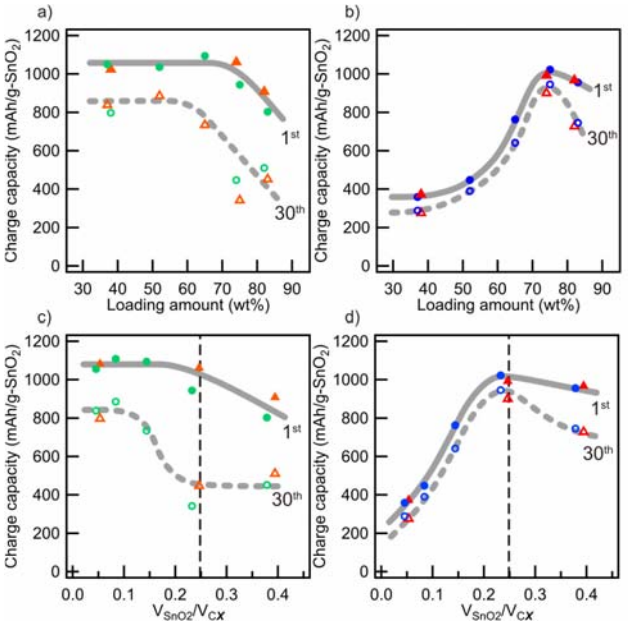

Figure 5. Relationship between charge capacities of SnO_2/C*X*[*w*] samples and structural parameters of (a, b) loading amount of SnO_2 and (c, d) the pore occupancy ratio by SnO_2 in the pore of C*X* (V_{SnO2}/V_{CX}) in OLE and ASS systems; (a, c) OLE system, (b, d) ASS system. The charge capacities at 1st and 30th cycle based on the weight of SnO_2. The vertical dashed line in (c) and (d) indicate the theoretical volume ratio of 24.6 v/v% (see text). The symbols are the same as those in Figure 4 (c, d).

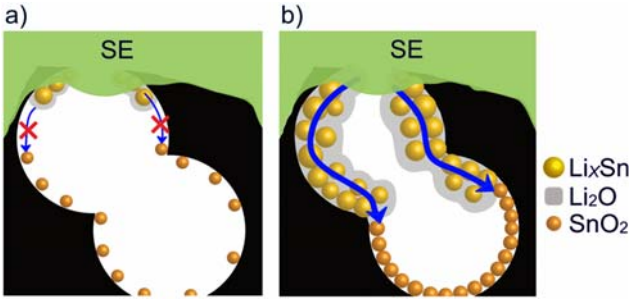

Figure 6. Schematic images of Li ion conduction in carbon nanopore of SnO_2/C*X*[*w*] samples; (a) low and (b) high SnO_2 loading. The blue arrow means Li-ion conduction path.

expansion accompanied with Sn-Li alloying and SnO_2-Sn conversion reactions is suppressed in such electrode to cause lowering the reactivity of active material at high constraint pressure.[9] In contrast, SnO_2/C140[75] showed the increase in capacity and coulombic efficiency with the increase in constraint pressure to 9.1 MPa. This means that the carbon nanopores in SnO_2/C140 act as a reaction buffer space for the volume expansion accompanying with charge-discharge reactions. It is considered that the capacity and coulombic efficiency of SnO_2/C140[75] are improved with the increase in constraint pressure, because the close SE/electrode interface can be maintained even under high confining pressure. The structures of carbon pore and SnO_2 inside the pore before and after lithiation were confirmed by using a simplified ASS half-cell composed of SnO_2/C*X*[*w*] without mixing SE as a working electrode. The XPS spectra of SnO_2/C45[74] suggested that SnO_2 can react

with Li ions even in the simplified ASS cell (Figure S6 in Supporting Information). The cross-section SEM images were taken against a working electrode of SnO_2/C140[65] in the simplified ASS cell (Figure S7 in Supporting Information). The macropore structure of C140 is maintained, and the embedded SnO_2 particles are not come outside of porous carbon before and after lithiation. The entire volume change of SnO_2/C*X*[*w*] composites seems to be suppressed due to presence of the buffer space for SnO_2 expansion. 9.1 MPa of external pressure at which the external pressure dependence test has shown highest capacity (Figure 3) was applied in the subsequent charge-discharge test.

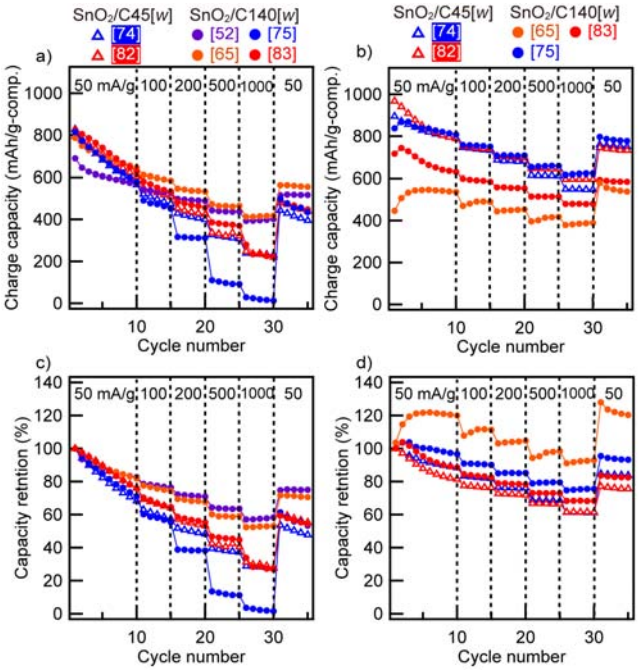

Figure 7. Capacity retention of SnO_2/C45[*w*] (open triangle) and SnO_2/C140[*w*] (closed circle) in (a, c) OLE and (b, d) ASS systems as functions of cycle number and specific current. The measurements were carried out at 50 mA/g-SnO_2 for the initial 10 cycles, and then at 100, 200, 500 and 1000 mA/g-SnO_2. The final five cycles were measured at 50 mA/g-SnO_2. The external consistent pressure on ASS system is 9.1 MPa. The numeral in brackets indicates the *w* value in SnO_2/C*X*[*w*].

3.3 Comparison of charge-discharge properties between in the ASS system and in the OLE system. In order to clarify the usability of porous carbon electrodes on the ASS system, the charge-discharge performances were compared with that of the OLE system. Figure 4(a) and (b) show charge capacities based on the composite weight of SnO_2/C*X*[*w*] as a function of cycle number up to 30 cycles in ASS and OLE systems. The initial charge capacity in OLE system was increased proportional to the SnO_2-loading amount up to around 70 wt% and then it was dropped over 75 wt% (Figure 4c) as previously reported.[11] On the other hand, the initial capacity in ASS system was increased dramatically with increasing *w* value up to around 70 wt%, and then was leveled off or decreased at $w > 75$ wt% (Figure 4d). The ASS system showed good cycle stability on the samples with $w < 70$ wt%, which is superior to OLE system. For example, the high capacity of SnO_2/C140[75] in ASS system was maintained with the retention of 99% even at 30th cycle (Figure 4b). We also confirmed the stable cycle performance up to 300 cycles on SnO_2/C140[75] at the specific current of 300 mA/g while keeping the high capacity; the capacity retention at 300th cycle was 97.4 % (Figure 4e).

The capacities of SnO_2/C*X*[*w*] based on the weight of SnO_2 in ASS and OLE systems were plotted against the *w* value and the pore space occupancy rate by SnO_2 in the pore of C*X* (V_{SnO_2}/V_{CX}) in Figure 5. The vertical dashed line in Figure 5(c, d) indicates the theoretical volume ratio of SnO_2 to pore volume of C*X* when the pores of C*X* are completely filled by $Li_{4.4}Sn$ and Li_2O. The SnO_2 volume is totally expanded 4.05 times with conversion reaction and alloying reaction (Supporting Information for the theoretical calculation). [18, 19] The charge capacity in OLE system was constant at $w < 70$, and was decreased steeply at $w > 70$ (Figure 5a), indicating low reactivity of SnO_2 in highly SnO_2-loaded composite. It is considered that sufficient reaction buffer space is needed for the volume change during reactions of SnO_2 with Li ions, since high capacity and better cyclability was observed in low V_{SnO_2}/V_{CX} region below the theoretical volume ratio in Figure 5c. In the case of ASS system, the capacity based on the weight of SnO_2 was increased with the increase in loading amount of SnO_2 up to around 75 wt% and with increasing V_{SnO_2}/V_{CX} up to the theoretical value (Figure 5b, d). The reactivity of SnO_2 in SnO_2/C*X*[*w*] is enhanced by the increase in its loading amount in the ASS system, of which behavior is quite different from that in the OLE system. The decrease in capacity and poor cyclability in high V_{SnO_2}/V_{CX} region above the theoretical volume ratio was observed even in the ASS system as in the OLE system.

In the OLE system, Li ions can easily access into the porous carbon through the OLE. However, in the ASS system where electrolyte is not present in the carbon pore, SE cannot migrate into the pore of C*X* unlike liquid electrolytes. The high capacities of ca.1000 mAh/(g-SnO_2) on SnO_2/C45[74] and SnO_2/C140[75] in the ASS system mean that any Li-ion conduction paths exists throughout the SnO_2-embedded carbon nanospace. There should be two possibilities of Li-ion conduction path, (1) through porous carbon or (2) via SnO_2 and Sn particles. In Figure 4 and 5, both of charge capacity based on the weight of composites and loaded SnO_2 were increased with the increase in the loading amount of SnO_2, whose profile is quite different from the OLE system. The profile implies that Li ions mainly conduct through SnO_2 and/or Sn in the carbon pores. The pore space occupancy rate by SnO_2 (V_{SnO_2}/V_{CX}) was 0.25 and 0.23 for SnO_2/C45[74] and SnO_2/C140[75], respectively. These values seem to be not enough for Li ion conduction through SnO_2 deposited in the nanopores of the composite without filling SE inside. The surface coverage of SnO_2 particle in porous carbon was calculated based on the closed packing layer structure of SnO_2 particles with the diameter of 3 nm. The particle size was determined from TEM images. The coverage of SnO_2 layer forming on meso or macropore surfaces was calculated to be 33-36% for SnO_2/C*X*[*w*] whose loading amount is ~75 wt%. The coverage is not enough that Li ion migrates via the loaded SnO_2 throughout nanopores in the sample without filling SE inside pores. However, after full lithiation of SnO_2 with totally 4.05 times volume expansion, the coverage is reached up to 71-76 % (detail calculation procedure in Supporting Information). The plausible Li-ion conduction model based

on the experimental and theoretical results is shown in Figure 6. Li-ion conduction paths should be formed in carbon nanospace of highly SnO_2-loaded samples during lithiation reactions accompanied with the large volume expansion. It is considered that Li-ion can migrate in carbon nanopores through Li_xSn and Li_xO which is lithiated phases of SnO_2. The Li conduction is limited near the pore mouths contacting with outside SE as for low SnO_2-loading samples. The gradually increase in capacity with cycling in early stage (Figure 3b) suggests the propagation of Li conduction area in the highly SnO_2-loaded sample and its electrode with the charge-discharge cycling.

Figure 7 shows rate capability of SnO_2/C*X*[*w*] in ASS and OLE systems, which was measured in the range of specific current from 50 mA/g to 1000 mA/g at room temperature. After 10 cycles of charging-discharging process at 50 mA/g, each 5 cycle was carried out at each specific current. Capacity retention was obtained by dividing the capacity by the initial capacity. Rate capability of low SnO_2-loading samples in the OLE system was much higher than that of high SnO_2-loading samples with high V_{SnO_2}/V_{CX} over the theoretical value. Although similar *w*-dependency on rate capability was observed, the rate performance of SnO_2/C*X*[*w*] in the ASS system was significantly higher than that in the OLE system. For example, SnO_2/C140[75] in the ASS system showed high rate capability, in which the retention even at high specific current of 1000 mA/g was over 75% against the capacity at 50 mA/g. Consequently, SnO_2-loading amount around 75wt% was the optimal condition to yield not only high capacity but also high rate capability while keeping cycle stability in ASS system among SnO_2/C*X*[*w*] samples prepared in this study.

4. Conclusion

The present study revealed that the SnO_2-embedded nanoporous carbons with an appropriate SnO_2-loading amount shows high capacity, high cycle stability and high rate performance in the ASS-LIB system superior to in the OLE-LIB system. It is important to design the nanopores in composite under considering buffer space for active materials which accompany large volume expansion during charge-discharge reaction. The buffer space plays an important role to suppress the volume expansion of electrode layer and to maintain a stable interface between SE and active material in the ASS system. The present approach is expected to be applied to other active materials which cause alloying-dealloying reaction or conversion reaction since Si, SiO_x and Ge-embedded porous carbons were developed as stable electrodes in OLE systems in recent years.[20, 21, 22] We could promise the extension of the high potential electrodes for next generation ASS batteries by optimization of composite structure and exploiting the compositional versatility.

ASSOCIATED CONTENT

Supporting Information.

The supporting information is available free of charge via the Internet at http://pubs.acs.org.

Equations and the explanation for calculations, XRD patterns of all samples, N_2 adsorption and desorption isotherm of all samples, pore size distribution of C45 and SnO_2/C45[*w*], TG curves of all samples, Charge-discharge curves and a d*Q*/d*V* curve of C140, XPS of SnO_2/C45[74] and SEM of SnO_2/C140[65] before and after 1st lithiation, Calculation of theoretical loading amount of SnO_2 from pore volume of C*X* and SnO_2/C*X*[*w*], Calculation of theoretical volume ratio of the full expanded state against original, Calculation of SnO_2 theoretical coverage of SnO_2 against pore surface of C*X*.

AUTHOR INFORMATION

Corresponding Author

*Isamu Moriguchi - *Graduate School of Engineering, Nagasaki University, 1-14 Bunkyo-machi, Nagasaki 852-8521, Japan,* Email: mrgch@nagasaki-u.ac.jp

Author Contributions

I.M. designed the research. H.N. and K.U. carried out the experiments and analyses. I.M., K.U., and H.N. evaluated the data. I.M. and H.N. prepared the manuscript.

ACKNOWLEDGMENT

This study made use of XRD and TEM in the Center for Instruments Analysis of Nagasaki University. This work was partly supported by JSPS KAKENHI Grant Numbers 18H02060, 20J12412.

REFERENCES

(1) Kato, Y.; Hori, S.; Saito, T.; Suzuki, K.; Hirayama, M.; Mitsui, A.; Yonemura, M.; Iba, H.; Kanno, R. High-Power All-Solid-State Batteries Using Sulfide Superionic Conductors. *Nat. Energy* **2016**, *1*, 16030.

(2) Minami, K.; Hayashi, A.; Tatsumisago, M. Mechanochemical Synthesis of Li_2S-P_2S_5 Glass Electrolytes with Lithium Salts. *Solid State Ionics* **2010**, *181* (33–34), 1505–1509. https://doi.org/10.1016/j.ssi.2010.08.021.

(3) Mizuno, F.; Hayashi, A.; Tadanaga, K.; Tatsumisago, M. New, Highly Ion-Conductive Crystals Precipitated from Li_2S-P_2S_5 Glasses. *Adv. Mater.* **2005**, *17* (7), 918–921. https://doi.org/10.1002/adma.200401286.

(4) Nagao, M.; Hayashi, A.; Tatsumisago, M. Fabrication of Favorable Interface between Sulfide Solid Electrolyte and Li Metal Electrode for Bulk-Type Solid-State Li/S Battery. *Electrochem. commun.* **2012**, *22* (1), 177–180. https://doi.org/10.1016/j.elecom.2012.06.015.

(5) Sakuda, A.; Hayashi, A.; Tatsumisago, M. Sulfide Solid Electrolyte with Favorable Mechanical Property for All-Solid-State Lithium Battery. *Sci. Rep.* **2013**, *3*, 2–6. https://doi.org/10.1038/srep02261.

(6) Winter, M.; Besenhard, J. O. Electrochemical Lithiation of Tin and Tin-Based Intermetallics and Composites. *Electrochim. Acta* **1999**, *45* (1), 31–50. https://doi.org/10.1016/S0013-4686(99)00191-7.

(7) Bucci, G.; Swamy, T.; Bishop, S.; Sheldon, B. W.; Chiang, Y.-M.; Carter, W. C. The Effect of Stress on Battery-Electrode Capacity. *J. Electrochem. Soc.* **2017**, *164* (4), A645–A654. https://doi.org/10.1149/2.0371704jes.

(8) Bucci, G.; Swamy, T.; Chiang, Y.-M.; Carter, W. C. Modeling of Internal Mechanical Failure of All-Solid-State Batteries during Electrochemical Cycling, and Implications for Battery Design. *J. Mater. Chem. A* **2017**, *5* (36), 19422–19430. https://doi.org/10.1039/C7TA03199H.

(9) Piper, D. M.; Yersak, T. A.; Lee, S.-H. Effect of Compressive Stress on Electrochemical Performance of Silicon Anodes. *J. Electrochem. Soc.* **2012**, *160* (1), A77–A81. https://doi.org/10.1149/2.064301jes.

(10) Oro, S.; Urita, K.; Moriguchi, I. Enhanced Charge–Discharge Properties of SnO_2 Nanocrystallites in Confined Carbon Nanospace. *Chem. Commun.* **2014**, *50* (54), 7143–7146. https://doi.org/10.1039/C4CC02716G.

(11) Oro, S.; Urita, K.; Moriguchi, I. Nanospace Control of SnO_2 Nanocrystallites-Embedded Nanoporous Carbon for Reversible Electrochemical Charge-Discharge Reactions. *J. Phys. Chem. C* **2016**, *120* (45), 25717–25724. https://doi.org/10.1021/acs.jpcc.6b09727.

(12) Shi, Y.; Liu, G.; Jin, R.; Xu, H.; Wang, Q.; Gao, S. Carbon Materials from Melamine Sponges for Supercapacitors and

Lithium Battery Electrode Materials: A Review. *Carbon Energy* **2019**, *1* (2), 253–275. https://doi.org/10.1002/cey2.19.

(13) Li, X.; Ni, J.; Savilov, S. V; Li, L. Materials Based on Antimony and Bismuth for Sodium Storage. *Chem. – A Eur. J.* **2018**, *24* (52), 13719–13727. https://doi.org/10.1002/chem.201801574.

(14) Notohara, H.; Urita, K.; Yamamura, H.; Moriguchi, I. High Capacity and Stable All-Solid-State Li Ion Battery Using SnO_2-Embedded Nanoporous Carbon. *Sci. Rep.* **2018**, *8* (1), 8747. https://doi.org/10.1038/s41598-018-27040-w.

(15) Kaneko, K.; Ishii, C. Superhigh Surface Area Determination of Microporous Solids. *Colloids and Surfaces* **1992**, *67* (C), 203–212. https://doi.org/10.1016/0166-6622(92)80299-H.

(16) Kaneko, K.; Cracknell, R. F.; Nicholson, D. Nitrogen Adsorption in Slit Pores at Ambient Temperatures: Comparison of Simulation and Experiment. *Langmuir* **1994**, *10* (12), 4606–4609. https://doi.org/10.1021/la00024a036.

(17) Otoyama, M.; Ito, Y.; Hayashi, A.; Tatsumisago, M. Raman Imaging for $LiCoO_2$ Composite Positive Electrodes in All-Solid-State Lithium Batteries Using Li_2S-P_2S_5 Solid Electrolytes. *J. Power Sources* **2016**, *302*, 419–425. https://doi.org/10.1016/j.jpowsour.2015.10.040.

(18) Patnaik, P. *Handbook of Inorganic Chemicals*; 2003. https://doi.org/10.1093/nq/s8-X.245.192c.

(19) $Li_{4.4}Sn$ ($Li_{17}Sn_4$) Crystal Structure: Datasheet from "PAULING FILE Multinaries Edition – 2012" in SpringerMaterials (Https://Materials.Springer.Com/Isp/Crystallographic/Docs/Sd_1601802). Springer-Verlag Berlin Heidelberg & Material Phases Data System (MPDS), Switzerland & National Institute for Materials Science (NIMS), Japan.

(20) Tabuchi, H.; Urita, K.; Moriguchi, I. Effect of Carbon Nanospace on Charge–Discharge Properties of Si and SiO_x Nanoparticles-Embedded Nanoporous Carbons. *Bull. Chem. Soc. Jpn.* **2015**, *88* (10), 1378–1384. https://doi.org/10.1246/bcsj.20150228.

(21) Tabuchi, H.; Nakamura, T.; Urita, K.; Moriguchi, I. Charge–Discharge Property of Si and SiO_x Nanoparticles Produced in Regulated Carbon Nanospace. *Chem. Lett.* **2014**, *44* (1), 23–25. https://doi.org/10.1246/cl.140862.

(22) Zeng, L.; Huang, X.; Chen, X.; Zheng, C.; Qian, Q.; Chen, Q.; Wei, M. Ge/GeO_2-Ordered Mesoporous Carbon Nanocomposite for Rechargeable Lithium-Ion Batteries with a Long-Term Cycling Performance. *ACS Appl. Mater. Interfaces* **2016**, *8* (1), 232–239. https://doi.org/10.1021/acsami.5b08470.

TOC

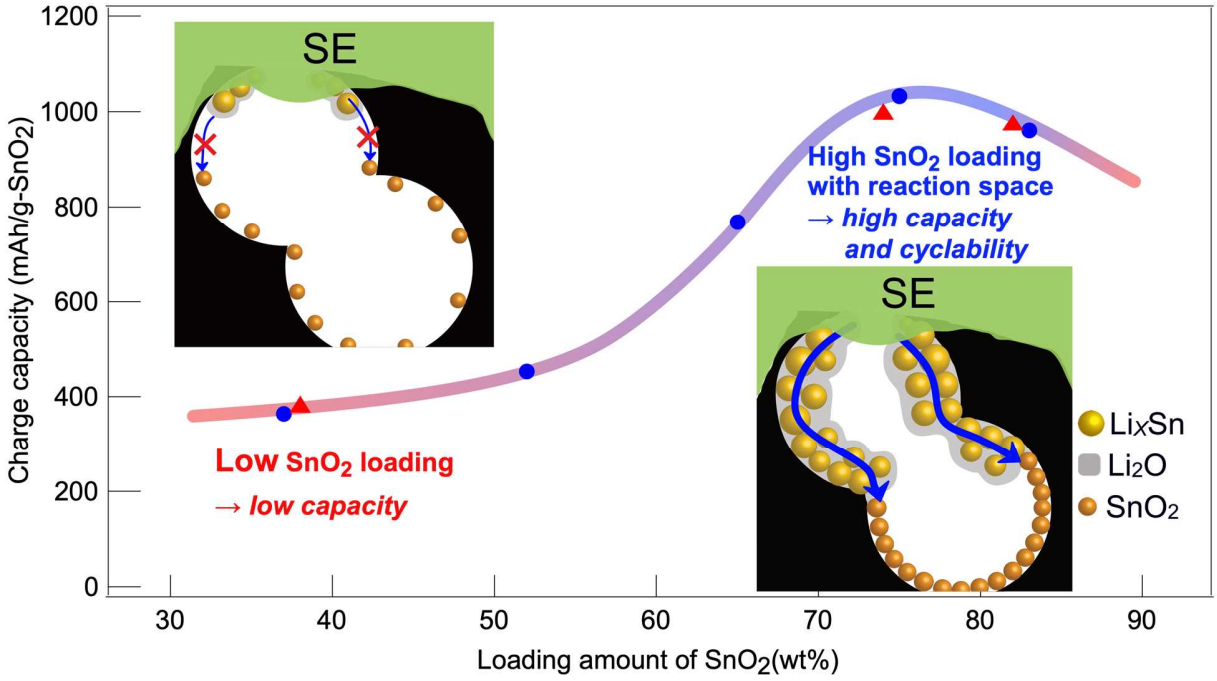
Charge capacity (mAh/g-SnO2)
1200
1000
800
600
400
200
0
30
40
50
60
70
80
90
Loading amount of SnO2(wt%)
SE
SE
High SnO2 loading
with reaction space
→ high capacity
and cyclability
Low SnO2 loading
→ low capacity
LixSn
Li2O
SnO2

Supporting Information for

SnO_2-embedded nanoporous carbon electrode with reaction-buffer space for stable all-solid-state Li ion battery

*Hiroo Notohara, Koki Urita, Isamu Moriguchi**

Graduate School of Engineering, Nagasaki University, 1-14 Bunkyo-machi, Nagasaki-shi, Nagasaki 852-8521, Japan.

*Corresponding Author: mrgch@nagsaki-u.ac.jp

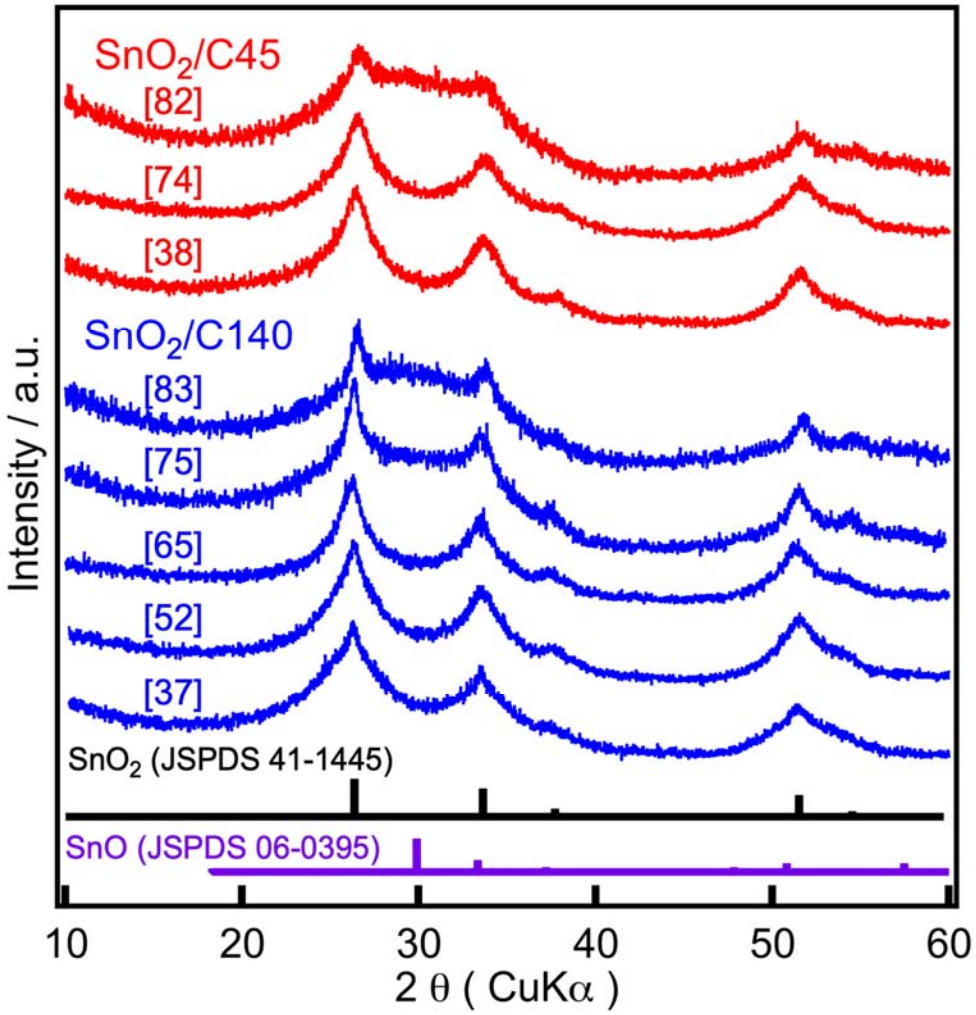

Figure S1. XRD patterns of the samples. [*w*] shows loading amount of SnO_2 in the samples. Low crystallinity SnO_2 and small amount of SnO should be formed at the samples with high loading amount. The crystallite size of SnO_2 is hardly changed and SnO generated from an inadequate hydrolysis reaction of $SnCl_2$ are formed with the increase in loading amount of $SnCl_2$. Since the loaded $SnCl_2$ particles are highly dispersed in the carbon pores for low loading amount composite, the hydrolysis reaction seems to be smoothly occurred. On the other hand, water or oxygen might partially react with densely packed $SnCl_2$ on the hydrolysis process; SnO nanoparticles were also generated in the high loading amount composites. Even though SnO nanoparticles were presence in the high loading amount composites, it was not critical reason for decreasing capacity and should not affect it as mentioned in previous study.[1)]

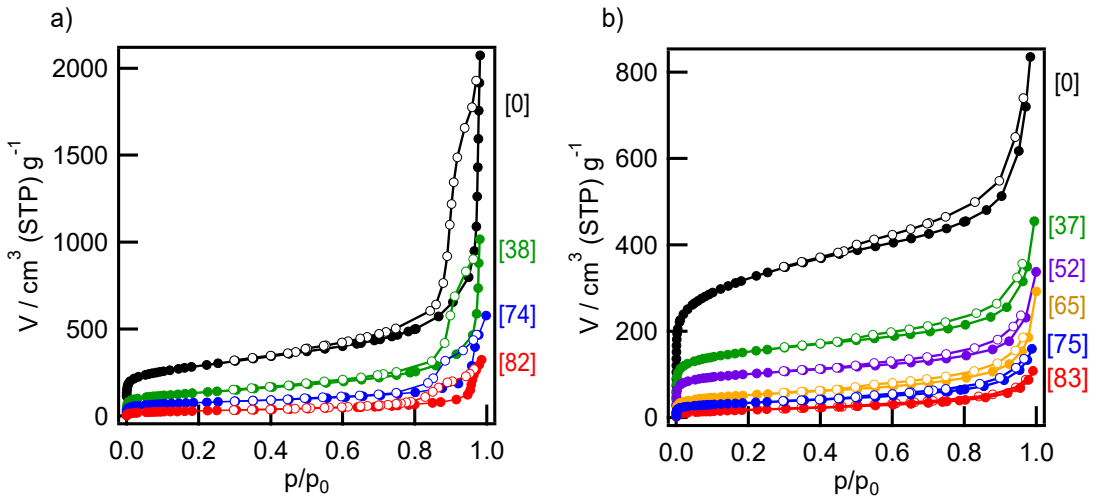

Figure S2. N_2 adsorption and desorption isotherm of (a) SnO_2/C45[*w*] and (b)SnO_2/C140[*w*]. Opened and closed circles indicate the value of adsorption and desorption, respectively. [*w*] shows loading amount of SnO_2 in the samples.

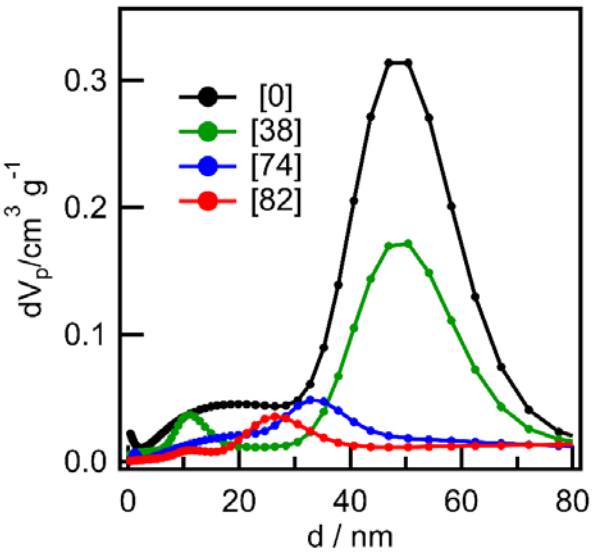

Figure S3. Pore size distribution of SnO_2/C45[*w*] determined from GCMC method against N_2 adsorption isotherm at 77 K in Fig. S4. [*w*] shows loading amount of SnO_2 in the SnO_2/C45 composites.

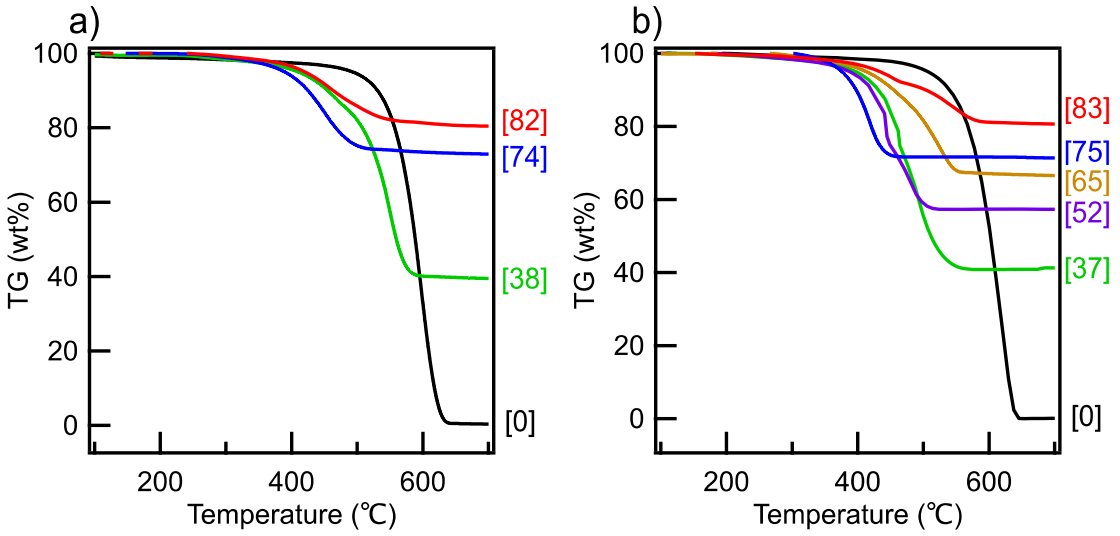

Figure S4. TG curves of (a) SnO_2/C45[*w*] and (b) SnO_2/C140[*w*]. [*w*] shows loading amount of SnO_2 in the samples. [*w*] shows loading amount of SnO_2 in the samples.

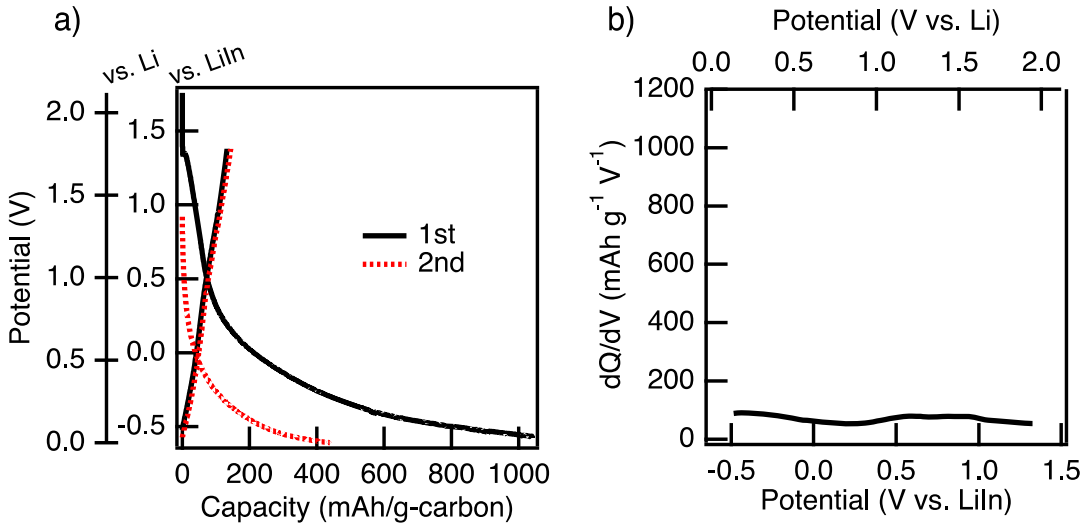

Figure S5. a) Charge-discharge curves and b) the dQ/dV curve of 1st charging process of C140 on the ASS system.

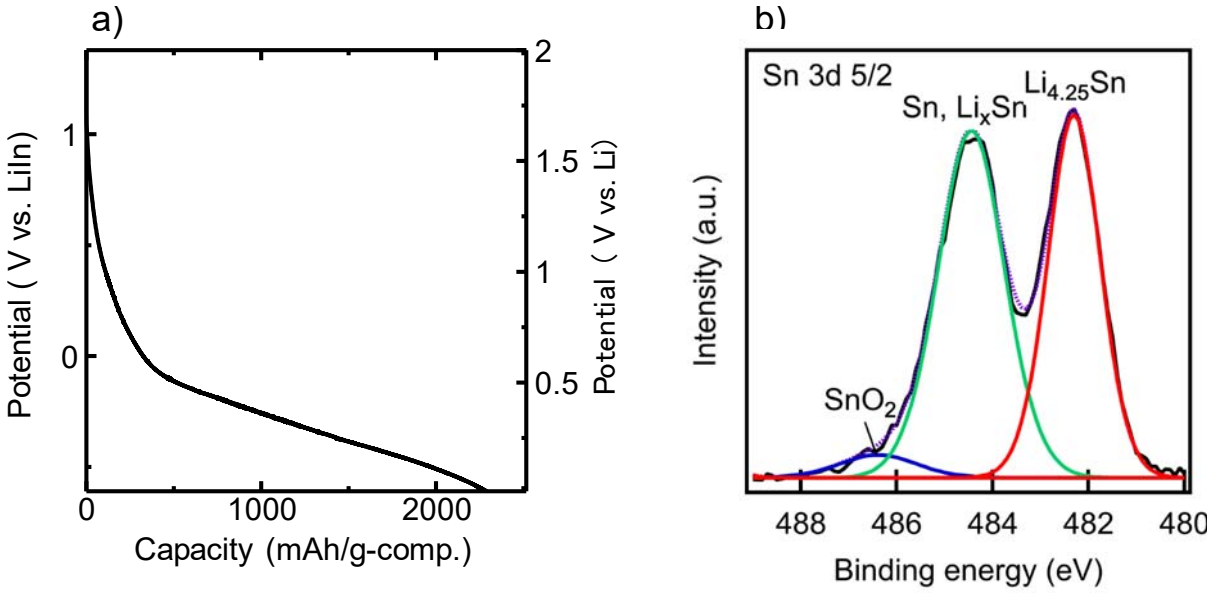

Figure S6. (a) An initial discharging curve of SnO_2/C45[74] measured on the simplified ASS system, in which a working electrode is not mixed with SE, (b) XPS spectra of Sn $3d_{5/2}$ of SnO_2/C45[74] after initial discharge. The ASS cell used here was consisted of SnO_2/C45[74], LiIn alloy and SE as the working electrode, the counter electrode and the electrolyte, respectively. The stacked three layers were sandwiched between two stainless-steel rods, which are current collectors, and then finally pressed at 200 MPa for 5 minutes at room temperature using a uniaxial oil hydraulic press. The discharging process was conducted at specific current of 50 mA/g-SnO_2 at 25°C. The peaks in XPS spectra were assigned from the data in previous report.[2) - 4)]

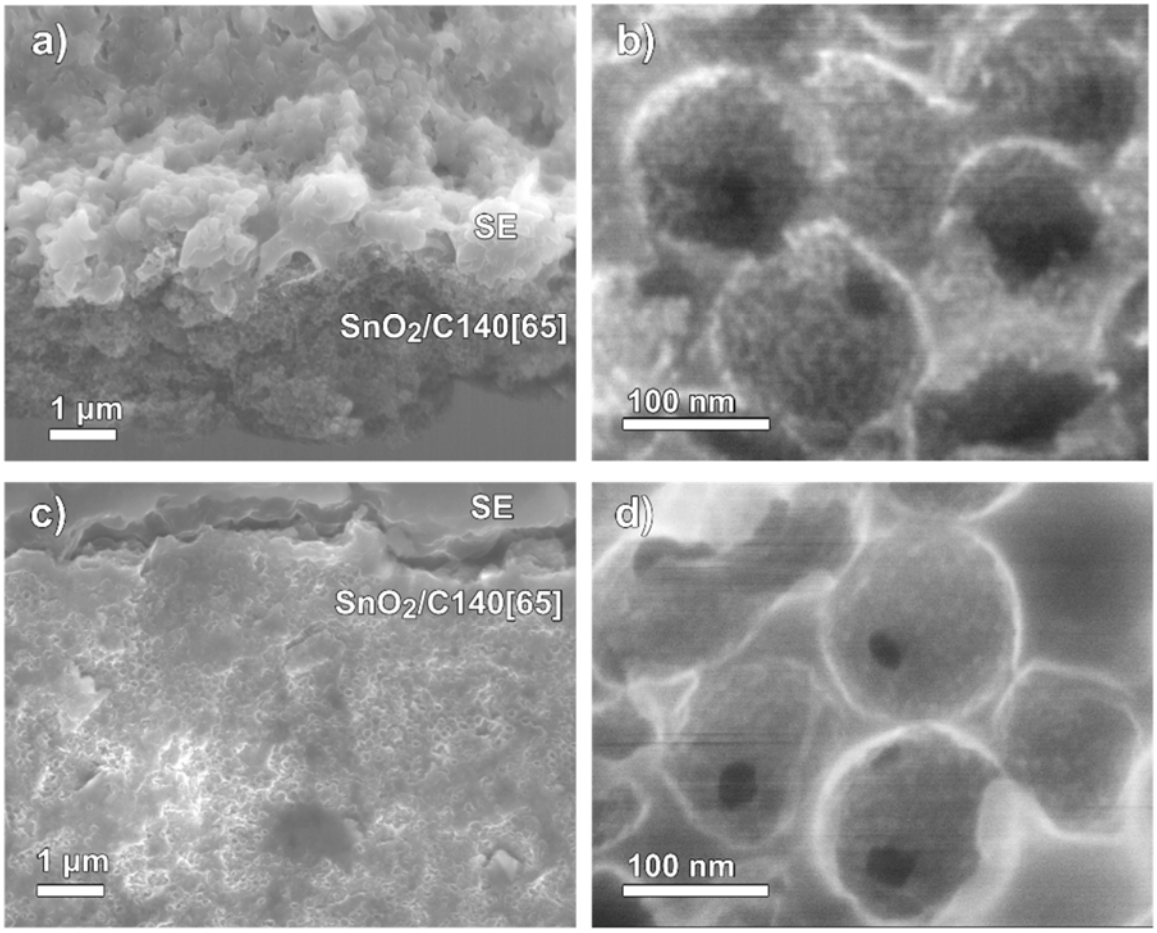

Figure S7. Cross-sectional SEM images of SnO_2/C140[65] (working electrode)//SE pellet (a, b) before and (c, d) after discharge process until -0.4 V vs. LiIn. The samples were obtained by splitting LiIn//SE//SnO_2/C140[65] pellet. The ASS test cell is same configuration with one used on XPS measurement. SnO_2 particles with diameter of ca. 5 nm are clearly observed on the surface of carbon pores before the discharge process. However, the obvious contrast derived from nanoparticles in carbon pores disappear after the discharge process (Fig. S7). Since the contrast in SEM images reflects the bumps and dips on the surface of samples, the smoothed surface of inner carbon pores strongly suggests coalescence of each SnO_2 nanoparticle due to volume expansion by reaction with Li ions, as mentioned in a previous report. [5] The porous structures are maintained even after lithiation. It suggests that the volume expansion of SnO_2 can proceed inside of the carbon pores, and the entire volume change of composite seems to be suppressed due to the presence of buffer space.

Supplementary Calculations

1. Theoretical loading amount of SnO_2 from pore volume of C*X* and SnO_2/C*X*[*w*]

The theoretical loading amount of SnO_2 ($W_{SnO2,\,calc}$) is calculated by using the following equations (1) and (2).

$$W_{SnO_2,calc.} = \frac{100x}{1+x} \qquad (1)$$

$$V_{comp} = \frac{V_C - x/\rho}{1+x} \qquad (2)$$

Where x is gram of SnO_2 per 1g of carbon in SnO_2/C*X*[*w*], V_{comp} and V_c are specific pore volume of the SnO_2/C*X*[*w*] and original C*X*, and ρ is the density of SnO_2 crystal (6.95 $cm^3\ g^{-1}$)[4], respectively.

2. Theoretical volume ratio of the full expanded state against original SnO_2

The theoretical volume ratio after the full reaction of SnO_2 with Li ions ([V_{expand}/V_{SnO2}]) is calculated to be 4.05 from the following equation (3):

$$\frac{V_{expand}}{V_{SnO_2}} = \frac{2\left(M_{Li_2O}/\rho_{Li_2O}\right)+\left(M_{Li_{4.4}Sn}/\rho_{Li_{4.4}Sn}\right)}{\left(M_{SnO_2}/\rho_{SnO_2}\right)} \qquad (3)$$

where M and ρ are molecular mass and density, respectively. The value of each material shown by subscript is as follows.

M_{SnO2} = 150.71 g mol^{-1}, ρ_{SnO2} =6.95 g cm^{-3} [6]

M_{Li2O} = 29.88 g mol^{-1}, ρ_{Li2O} = 2.01 g cm^{-3} [7]

$M_{Li4.4Sn}$ = 149.25 g mol^{-1}, $\rho_{Li4.4Sn}$ = 2.57 g cm^{-3} [8]

3. Theoretical coverage of SnO_2 against pore surface of C*X*

When spherical nanoparticles of SnO_2 with the diameter of 3 nm are closely packed and form a single layer over the whole surface of mesopores and macropores of C*X*, the theoretical coverage (θ) can be calculated by following equations (4), (5) and (6):

$$\theta = 100 \times S_{SnO_2} \Big/ S_C \tag{4}$$

$$S_{SnO_2} = \frac{y}{\left(\frac{4\pi}{3}\right)\left(\frac{d}{2}\right)\rho_{SnO_2}} \times 2\sqrt{3}\left(\frac{d}{2}\right)^2 \tag{5}$$

$$Y = \frac{100y}{1+y} \tag{6}$$

where S_i is a surface area of SnO_2 particle forming monolayer on the carbon pores (i = SnO_2) and specific surface area of meso or macropores of C*X* (i = C), y is gram of SnO_2 per 1g of carbon in SnO_2/C*X*[w] and d is particle diameter of SnO_2, which is here 3 nm.

At the expansion state after the full reaction of SnO_2 with Li ions, the coverage (θ_{expand}) is expressed by equations (7) and (8):

$$\theta_{expand} = 100 \times S_{expand} \Big/ S_C \tag{7}$$

$$S_{expand} = 4.05^{2/3} \times S_{SnO_2} \tag{8}$$

where S_{expand} is the total surface area of $Li_{4.4}Sn$ and Li_2O after the full reaction with Li ions.

Supporting references

1) Oro, S.; Urita, K.; Moriguchi, I. Nanospace Control of SnO_2 Nanocrystallites-Embedded Nanoporous Carbon for Reversible Electrochemical Charge-Discharge Reactions. *J. Phys. Chem. C* **2016**, *120* (45), 25717–25724. https://doi.org/10.1021/acs.jpcc.6b09727.
2) Böhme, S.; Philippe, B.; Edström, K.; Nyholm, L. Photoelectron Spectroscopic Evidence for Overlapping Redox Reactions for SnO_2 Electrodes in Lithium-Ion Batteries. *J. Phys. Chem. C* **2017**, *121* (9), 4924–4936. https://doi.org/10.1021/acs.jpcc.7b01529.
3) Ferraresi, G.; Villevieille, C.; Czekaj, I.; Horisberger, M.; Novák, P.; El Kazzi, M. SnO_2 Model Electrode Cycled in Li-Ion Battery Reveals the Formation of Li_2SnO_3 and Li_8SnO_6 Phases through Conversion Reactions. *ACS Appl. Mater. Interfaces* **2018**, *10* (10), 8712–8720. https://doi.org/10.1021/acsami.7b19481.
4) Ding, J.; Li, Z.; Wang, H.; Cui, K.; Kohandehghan, A.; Tan, X.; Karpuzov, D.; Mitlin, D. Sodiation vs. Lithiation Phase Transformations in a High Rate – High Stability SnO_2 in Carbon Nanocomposite. *J. Mater. Chem. A* **2015**, *3* (13), 7100–7111. https://doi.org/10.1039/C5TA00399G.
5) Ali, G.; Patil, S. A.; Mehboob, S.; Ahmad, M.; Ha, H. Y.; Kim, H. S.; Chung, K. Y. Determination of Lithium Diffusion Coefficient and Reaction Mechanism into Ultra-Small Nanocrystalline SnO_2 Particles. *J. Power Sources* **2019**, *419* (January), 229–236. https://doi.org/10.1016/j.jpowsour.2019.02.052.
6) *CRC Handbook of Chemistry and Physics*; Lide T. D. ed.; 75th edition; CRC press inc.; Boca Raton, **1994**.
7) Patnaik, P. *Handbook of inorganic chemicals*; McComb, K. ed.; The McGraw-Hill Companies, Inc.; New York, **2003**.
8) Gladyshevskii, E. I.; Oleksiv, G. I.; Kripyakevich, P. I. New Examples of the Structural Type $Li_{22}Pb_5$. *Sov. Phys. Crystallogr*. **1964**, *9*, 269-271.